Mechanics & Industry **20**, 622 (2019)
© AFM, EDP Sciences 2019
https://doi.org/10.1051/meca/2019055

Mechanics & Industry

Available online at:
www.mechanics-industry.org

Regular Article

Investigation into the dynamic characteristics of downhole perforation tools with multiple shock absorbers

Xiaoqiang Guo[1,*], Jun Liu[1,2], Guorong Wang[1,2], Qingyou Liu[3], and Xianming Song[4]

[1] School of Mechatronic Engineering, Southwest Petroleum University, Chengdu, 610500, PR China
[2] Energy Equipment Institute of Southwest Petroleum University, Chengdu 610500, PR China
[3] Chengdu University of Technology, Chengdu 610059, PR China
[4] Drilling Technology Research Institute of Jidong Oilfield Company, Tangshan 063000, PR China

Received: 17 February 2019 / Accepted: 19 July 2019

Abstract. The use of large-charged perforating bullets after well perforation produces large impact loads, which can easily lead to early unsealing of packers, damage to testing instruments, stress failure of tubing strings, buckling deformation, and other adverse incidents. This study focuses on the safety of large-charged perforating bullets used in downhole tools. In addition, a dynamic model of downhole perforation tools with multi-shock absorber was designed, and ANSYS software was used to validate its accuracy. Perforation impact loading field experiments were developed, and the loading pressure was measured over time to obtain an even more accurate equation to calculate loading. Analysis of the effects of different numbers of shock absorbers on the dynamic characteristics of downhole tools was conducted, finding that increasing the number of shock absorbers from one to two significantly decreased the dynamic response amplitude of the downhole tools (displacement, axial force, and packer force). However, when the number was increased to three, the change in response amplitude was not significant. Based on the maximum acceleration of each section of the tubing string, the testing instrument is best installed at its upper end. As the number of shock absorbers is increased, the number of regions of the tubing string that undergo buckling deformation decreases. Increasing the number of shock absorbers helps prevent buckling deformation in the tubing string, and increases its service life.

Keywords: Perforation / downhole tools / dynamic model / shock absorber settings / impact load

1 Introduction

After well perforation, high perforation density and perforating bullets with high explosive charge are widely used, due to the diversity of downhole tools. Figure 1 shows the complexity of the well structure shown by Liu et al. [1], which makes the whole mechanical environment very complex and harsh. Therefore, in order to reduce the incidence of packer failure caused by the large force, reduce the risk of damage caused by large acceleration of the test instrument, and avoid the occurrence of tubing string instability and damage, it is necessary to overcome the contradiction between higher perforation efficiency and lower perforation impact load on the tubing string.

Determining the impact load of perforation is the basis of dynamic analysis of the perforating tool. Ning [2] proposed based a method to calculate perforation load based on explosion theory, but its calculation precision is quite different from the actual engineering. In 2002, Ren et al. [3] carried out numerical simulation of an explosion in shallow water using ANSYS/LS-DYNA to obtain the pressure curve of the explosion, but they were unable to obtain the calculation formula for the explosion impact load. Thus, a similar experimental study on underwater explosions was carried out by Li et al. [4], who obtained the calculation formula for the explosion impact load, while however ignoring but the rising section of the impact load. Zhang et al. [5] presented a model to calculate perforation impact load and investigate the influence patterns law of different parameters on it. However, their formula of load calculation cannot be effectively applied to practical engineering. Lu et al. [6] studied the blast wave pattern in equal-aperture projectile explodes using numerical simulation and experiments, finding that detonation of an equal aperture perforation bomb had stronger penetrating capacity than that of conventional perforation. Pan et al. [7] investigated the perforation performance of perforated projectile double-layer explosive covers, finding that the perforation ability generated load of the double-layer charge with energy

* e-mail: 786526101@qq.com

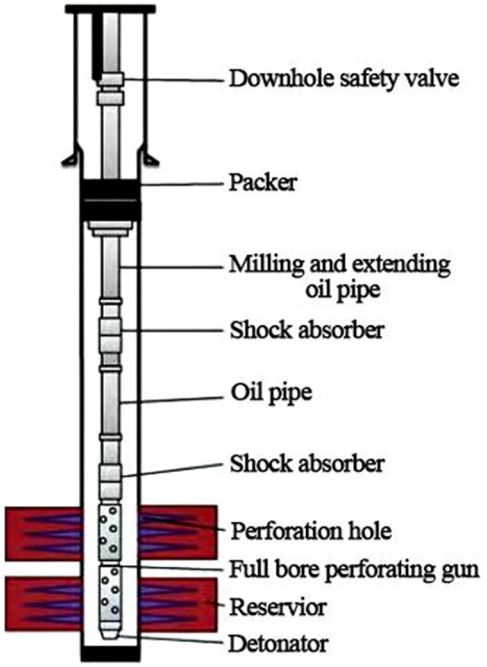

Fig. 1. Downhole tools in the perforation operation.

perforating projectiles was significantly higher than that of conventional perforating projectiles. Formulating the perforating load is however still a difficult problem. On the basis of previous research by Liu et al. [8], this paper further improves the calculation model of perforation load based on new field measurements of perforation pressure field data, bringing it closer to engineering practice.

Pipe string mechanics research forms some of the basic work of perforating tool combination design. Various studies since 1953 Lubinski et al. [9,10] have successively studied the stability of the string and presented critical load formulas of its initial sinusoidal buckling and the helical buckling, considering the continuous contact between the pipe string and the casing. Sorenson et al. [11] studied the mechanical behavior of the buckling string, considering the uneven contact between the buckling pipe string and well wall, and the friction between the pipe string and pipe wall. Their work established a corresponding mechanical model, obtaining the force and deformation of the buckling string. In 2008, Cui et al. [12] investigated the dynamic response in perforation of ultra-deep wells based on the assumption of infinite length pipe, with the upper end fixed, and the lower end connected by a single shock absorber. Although their model can calculate axial deformation and force along the string direction, the assumption of infinitely long pipe strangle is not realistic. Methods to reduce the impact of perforation shock vibration are discussed in Chen et al. [13], analyzing the effect of perforation impact load on the ultra-deep pipe string wells during the combined perforation-test-acidification combination, using empirical formulas and numerical simulation. Li et al. [14] established a mechanical model to analyze the tension, torque, stress, safety factor, and stability of the whole string during formation tests. Yang et al. [15] used thermodynamics theory to study the influence of different perforating explosion parameters on the perforation impact load safety of the pipe string, providing theoretical guidance for the pipe string design. Using the working mechanism of perforation pipe strings, Zhou [16] investigated dynamic response of perforating pipe string under impact load by means of experiment and mechanical simulation. Huang [17] established a longitudinal vibration dynamic model for the testing tube and shock absorber to study the influence of perforation parameters on the dynamic characteristics of the pipe string and packer. His model ignored the effects of shock absorber quality. In 2016, Gao Deli et al. [18–20] proposed mechanical models from no buckling to plane buckling, and plane buckling to helical buckling. Li et al. [21] expounded upon the future direction of research on string mechanics in oil and gas wells and corresponding research methods, indicating directions for future research. In 2017–2019, Scholars (Ke et al. [22], Feng et al. [23,24], Nguyen et al. [25]) presented dynamics model of drill-string and investigate the dynamic characteristics of drill-string the factors of structure parameter. At present, there is no report on the dynamics of perforated pipe string with multiple shock absorbers.

Research on perforating string mechanics mainly focuses on buckling deformation analysis and static analysis of the tubing string. Dynamic analysis of the downhole tool is still based on the simplified model of Cui et al. [12], or the single shock absorber model by Liu et al. [8]. With the increasing strength of perforating impact load, the downhole tools are being combined with multiple shock absorbers more and more frequently, therefore analysis of their dynamic characteristics is becoming necessary. On the basis of the previous research by Liu et al. [8] on the dynamics of perforation tubing string with a single shock absorber, this paper further optimizes the perforation load calculation model based on new experimental data, and extends the dynamic tubing string model with one shock absorber to multiple shock absorbers. Based on this, the influence mechanism of shock absorber configuration on the dynamic response of the pipe string is discussed, providing theoretical support for the design of perforation tool combinations with large charge.

2 A dynamic model of downhole tools with multiple shock absorbers

2.1 Basic assumptions

Based on the structure and perforation process analysis of the downhole perforation tools, before establishing the downhole perforation tool dynamic model, some basic assumptions were made as follows:

- A shock absorber is equivalent to a mass-spring-damping system.
- The materials of the tubing string and perforation gun are uniform and isotropic.
- The packer is considered as a fixed abutment, irrespective of the relative displacement between it and the casing or tubing string.

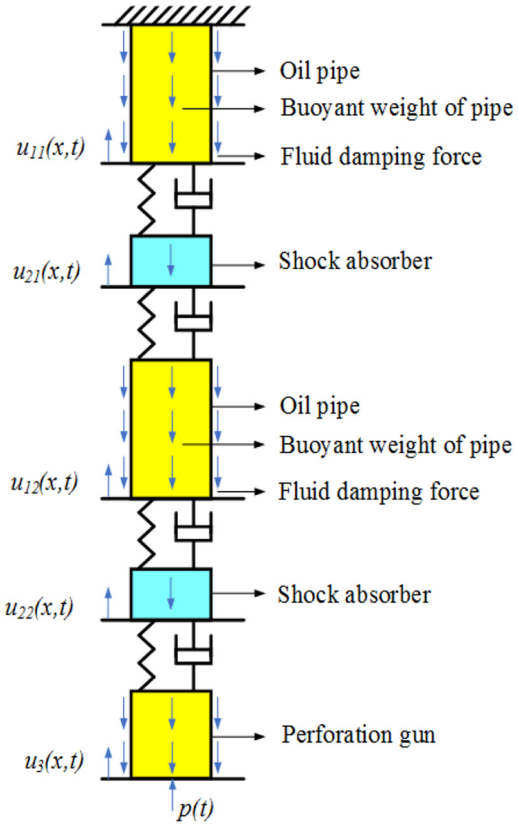

Fig. 2. Dynamic model of oil pipe-shock absorber-perforation gun (two shock absorbers).

– Only the longitudinal vibration of the tubing string is considered, ignoring vibrations in other directions.

2.2 Differential vibration equation of the downhole tool

Based on the above basic assumptions, the vibration differential equation of a downhole tool with two shock absorbers is established. The dynamic model is depicted in Figure 2.

2.2.1 Differential vibration equation of perforation tube

In joint perforation and testing, the perforation tube mainly includes tubing string, perforation gun and casing. Considering the tubing string and the perforation gun as the same type of tubular column, the differential method and d'Alembert principle are used to establish the equations governing the tubular column. The specific process is described in the literature by Liu et al. [8], and the following equation can be obtained.

$$\rho A_0 \frac{\partial^2 u_1}{\partial t^2}\mathrm{d}x + E_0 A_0 \frac{\partial u_1}{\partial x} + v\frac{\partial u_1}{\partial t}\mathrm{d}x - \left(E_0 A_0 \frac{\partial u_1}{\partial x} + \frac{\partial}{\partial x}\left(E_0 A_0 \frac{\partial u_1}{\partial x}\right)\mathrm{d}x\right) - \rho g A_0 \mathrm{d}x = 0, \quad (1)$$

where $\mathrm{d}x$ is the length differential, E_0 is the elastic modulus of the tubing string, A_0 is the cross-section area of the tubing string, ρ is density, and u_1 is the displacement of micro segment of tubing string.

After transformation of formula (1), the partial vibration differential equation of the perforation tube is obtained as follows.

$$\frac{\partial^2 u_1}{\partial t^2} - a^2\frac{\partial^2 u_1}{\partial x^2} + v\frac{\partial u_1}{\partial t} = g, \quad (2)$$

where a is the wave propagation speed in the tube, $a = \sqrt{E_0/\rho}$, g is the constant obtained by simplifying the perforation tube weight, $\rho A_0 g_0$, and v is the damping coefficient on the perforation tube between the liquid on its inside and outside.

2.2.2 Coupling conditions for tubing string-shock absorbers-perforation gun (two shock absorbers)

The schematic diagram of the downhole tool dynamic model shows that the model has two coupling boundaries (oil pipe-shock absorber-oil pipe and oil pipe-shock absorber-perforation gun), based on the action of two shock absorbers. Coupling boundaries require force continuity conditions. Based on the above, we can conclude that the six coupling equations are as follows. For detailed derivations, refer to Liu et al. [8].

– The continuity equation of the lower end force of the tubing string is

$$E_0 A_0 \frac{\mathrm{d}u_{1i}}{\mathrm{d}x} = c_i \frac{\mathrm{d}}{\mathrm{d}t}[u_{1i}(t) - u_{2i}(t)] + k_i[u_{1i}(t) - u_{2i}(t)] + m_{oe}\frac{\mathrm{d}^2 u_{1i}}{\mathrm{d}t^2}, \quad i = 1, 2 \quad (3)$$

where $u_{1i}(t)$ is the displacement of the lowermost portion of tubing string, $u_{2i}(t)$ is the displacement of the shock absorber, m_{oe} is the mass of the tubing string micro-segment, k_i is the stiffness coefficient of the shock absorber, and c_i is the damping coefficient of the shock absorber.

– The continuity equations of force on the shock absorber are

$$c_1\frac{\mathrm{d}}{\mathrm{d}t}[u_{11}(t) - u_{21}(t)] + k_1[u_{11}(t) - u_{21}(t)] = m_{p_1}g + m_{p_1}\frac{\mathrm{d}^2 u_{21}}{\mathrm{d}t^2} + c_1\frac{\mathrm{d}}{\mathrm{d}t}[u_{21}(t) - u_{12}(t)] + k_1[u_{21}(t) - u_{12}(t)] \quad (4a)$$

$$c_2\frac{\mathrm{d}}{\mathrm{d}t}[u_{12}(t) - u_{22}(t)] + k_2[u_{12}(t) - u_{22}(t)] = m_{p_2}g + m_{p_2}\frac{\mathrm{d}^2 u_{22}}{\mathrm{d}t^2} + c_2\frac{\mathrm{d}}{\mathrm{d}t}[u_{22}(t) - u_3(t)] + k_2[u_{22}(t) - u_3(t)] \quad (4b)$$

where m_{p_1} is the mass of the first shock absorber, and $u_3(t)$ is the displacement of the end of the perforation gun.

– The continuity equation of the force on the upper end of the second tubing string is

$$c_1\frac{\mathrm{d}}{\mathrm{d}t}[u_{21}(t)-u_{12}(t)]+k_1[u_{21}(t)-u_{12}(t)] = m_{oe}\frac{\mathrm{d}^2u_{12}}{\mathrm{d}t^2}+E_0A_0\frac{\mathrm{d}u_{12}}{\mathrm{d}x}. \quad (5)$$

– The continuity equation of the force on the top end of the perforation gun is

$$c_2\frac{\mathrm{d}}{\mathrm{d}t}[u_{22}(t)-u_3(t)]+k_2[u_{22}(t)-u_3(t)] = m_{pe}\frac{\mathrm{d}^2u_3}{\mathrm{d}t^2}+E_pA_p\frac{\mathrm{d}u_3}{\mathrm{d}x} \quad (6)$$

where m_{pe} is the differential segment mass of the perforation gun, E_p is the elastic modulus of the perforation gun, and A_p is the cross-sectional area of the perforation gun.

– The equation of forces on the lower end of the perforation gun is

$$p_{(t)} = E_pA_p\left.\frac{\mathrm{d}u_{3d}}{\mathrm{d}x}\right|_{x=l}+m_{pe}\frac{\mathrm{d}^2u_{3d}}{\mathrm{d}t^2}+m_{pe}g \quad (7)$$

where u_{3d} is the displacement of the bottom of the perforation gun, and $p_{(t)}$ is the impact load of the perforation gun.

2.2.3 Oil pipe-shock absorbers-perforation gun (three shock absorber) coupling conditions

The model of the three shock absorbers connected to the perforated tubing string is shown in Figure 3; the model construction method is the same as that for two shock absorbers. The control equation is extended based on the original model, so the description will not be repeated.

2.3 Solving the dynamic model

The equations are solved using finite differences according to the differential equations (2)–(7). The discretized formulae are obtained as follows, with reference by Huang [17].

See Equations (8a) to (8h) below.

$$u_{i,j+1} = \frac{\frac{a^2\Delta t^2}{\Delta x^2}\left(u_{i+1,j}+u_{i-1,j}\right)-\left(2\frac{a^2\Delta t^2}{\Delta x^2}-2.0-v\Delta t\right)u_{i,j}-u_{i,j-1}+g\Delta t^2}{1+v\Delta t} \quad (8a)$$

$$E_0A_0\frac{u_{i,j+1}-u_{i+1,j+1}}{\Delta x}=c_1\left(\frac{u_{i+1,j+1}-u_{i+2,j+1}}{\Delta t}-\frac{u_{i+1,j}-u_{i+1,j}}{\Delta t}\right)+k_1\left(u_{i+1,j+1}-u_{i+2,j+1}\right)+m_{oe}\frac{u_{i+1,j+1}-2u_{i+1,j}+u_{i+1,j-1}}{\Delta t^2} \quad (8b)$$

$$c_1\left(\frac{u_{i+1,j+1}-u_{i+2,j+1}}{\Delta t}-\frac{u_{i+1,j}-u_{i+1,j}}{\Delta t}\right)+k_1\left(u_{i+1,j+1}-u_{i+2,j+1}\right)=m_{p_1}g+m_{p_1}\frac{u_{i+2,j+1}}{\Delta t^2}-\frac{2u_{i+2,j}-u_{i+2,j-1}}{\Delta t^2}$$
$$+c_1\left(\frac{u_{i+2,j+1}-u_{i+3,j+1}}{\Delta t}-\frac{u_{i+2,j}-u_{i+3,j}}{\Delta t}\right)+k_1\left(u_{i+2,j+1}-u_{i+3,j+1}\right) \quad (8c)$$

$$c_1\left(\frac{u_{i+2,j+1}-u_{i+3,j+1}}{\Delta t}-\frac{u_{i+2,j}-u_{i+3,j}}{\Delta t}\right)+k_1\left(u_{i+2,j+1}-u_{i+3,j+1}\right)=m_{oe}\frac{u_{i+3,j+1}-2u_{i+3,j}+u_{i+3,j-1}}{\Delta t^2}$$
$$+E_0A_0\frac{u_{i+3,j+1}-u_{i+4,j+1}}{\Delta x} \quad (8d)$$

$$E_0A_0\frac{u_{i+n+2,j+1}-u_{i+n+3,j+1}}{\Delta x}=c_2\left(\frac{u_{i+n+3,j+1}-u_{i+n+4,j+1}}{\Delta t}-\frac{u_{i+n+3,j}-u_{i+n+4,j}}{\Delta t}\right)+k_2\left(u_{i+n+3,j+1}-u_{i+n+4,j+1}\right)$$
$$+m_{oe}\frac{u_{i+n+3,j+1}-2u_{i+n+3,j}+u_{i+n+3,j-1}}{\Delta t^2} \quad (8e)$$

$$c_2\left(\frac{u_{i+n+3,j+1}-u_{i+n+4,j+1}}{\Delta t}-\frac{u_{i+n+3,j}-u_{i+n+4,j}}{\Delta t}\right)+k_2\left(u_{i+n+3,j+1}-u_{i+n+4,j+1}\right)=m_{p_2}g+m_{p_2}\frac{u_{i+n+4,j+1}}{\Delta t^2}$$
$$-\frac{2u_{i+n+4,j}-u_{i+n+4,j-1}}{\Delta t^2}+c_2\left(\frac{u_{i+n+4,j+1}-u_{i+n+5,j+1}}{\Delta t}-\frac{u_{i+n+4,j}-u_{i+n+5,j}}{\Delta t}\right)+k_2\left(u_{i+n+4,j+1}-u_{i+n+5,j+1}\right) \quad (8f)$$

$$c_2\left(\frac{u_{i+n+4,j+1}-u_{i+n+5,j+1}}{\Delta t}-\frac{u_{i+n+4,j}-u_{i+n+5,j}}{\Delta t}\right)+k_1\left(u_{i+n+4,j+1}-u_{i+n+5,j+1}\right)$$
$$=m_{pe}\frac{u_{i+n+5,j+1}-2u_{i+n+5,j}+u_{i+n+5,j-1}}{\Delta t^2}+E_pA_p\frac{u_{i+n+5,j+1}-u_{i+n+6,j+1}}{\Delta x} \quad (8g)$$

$$p_{(t)} = E_pA_p\frac{u_{(np+2+np1+1,j+1)}-u_{(np+2+np1,j+1)}}{l_{pe}}+m_{pe}\frac{u_{(np+2+np1+1,j+1)}-2u_{(np+2np1+1,j)}+u_{(np+2+np1+1,j-1)}}{\Delta t^2}+m_{pe}g. \quad (8h)$$

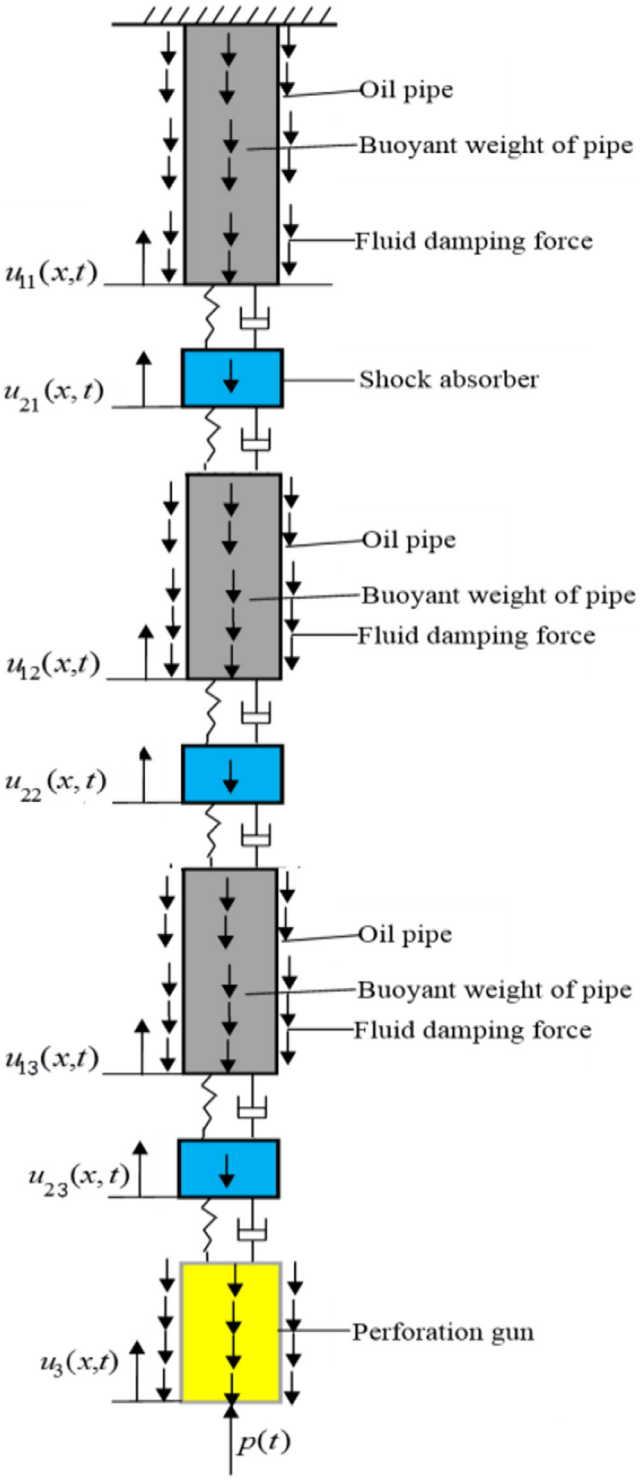

Fig. 3. Dynamic oil pipe-shock absorber-perforation gun (three shock absorber) model.

These eight discrete equations do not yet solve the displacement of each node of the tubular column. The boundary conditions of force and displacement are also required, so they will be introduced next.

2.4 Model boundary conditions and convergence conditions

Since the upper end of the tubing string is connected to the packer, the forces acting upon each body interact. Assuming that the packer is fixed, then the upper end of the tubing string is fixed as $u_{1u}(0, t) = 0$; assuming that the bottom of the perforation gun bears the perforation load, the bottom end of the tubular column system can be expressed as $E_r A_r \frac{\partial u}{\partial x}|_{x=L} = P_p(t)$.

Finally, by introducing the boundary conditions, the displacement curves of the various sections for the tubular column over time can be calculated. In the process of solving the wave equation using the differential method, however, problems of stability and convergence emerge. Huang [17] cites the convergence condition of finite difference decomposition of wave equations, i.e. that the coefficient of $u_{i,j}$ is non-negative. The coefficients from equation (11) (i.e. the convergence conditions to solve the wave equation through the differential method) are as follows.

$$1 - \frac{a^2 \Delta t^2}{\Delta x^2} \geq 0. \tag{9}$$

3 Field tests of perforation impact load

3.1 The purpose and equipment of the field experiment

3.1.1 Purpose of the field experiment

In order to calculate the impact load of perforation explosion, most scholars [8,14,17] adopt the formula to calculate explosive load in free water. Its accuracy does not meet the requirements for actual perforation explosion calculation results. Therefore, in this paper, a well of CNOOC is selected to carry out field experimental research on the calculation of perforation explosion impact load, and finds a more accurate formula for impact load. The next section provides precise boundary conditions for the analysis of vibration characteristics of downhole perforation tools, laying a foundation for the field reliability of the results in this paper.

3.1.2 Equipment used

The field experiment was configured as follows. A 114 external composite perforation device was used for external composite perforation. The transmission method was workover rig oil pipe transportation, using a sealer. The sand II and III oil layer positions were divided into two perforations. In the middle and tail end of the perforation tube, a downhole high-speed manometer was used to collect real-time data on the gunpowder explosions. The specific perforation equipment is shown in Table 1, and the basic structure of the operational tube is displayed in Figure 4.

Table 1. Perforation equipment list.

Name	Parameters
114 perforating gun	Length: 4.5 m, Shot density: 16 spm, Phase: 60° levoclination, Compression: 130 Mpa, Tensile: 140 000 kg, Weight: 29 kg/m
Ignition cable switch	Type: YBK2-1-HY, Compression: 120 MPa
Pipe string	2-7/8″ EUE oil pipe, External diameter: 93 mm, Internal diameter: 57 mm, Tension: 846 kN
Perforating bullets	Type: 692SD-114H-3, Charge: 39 g, Penetration: 1541.5 mm, Bore diameter: 11.2 mm

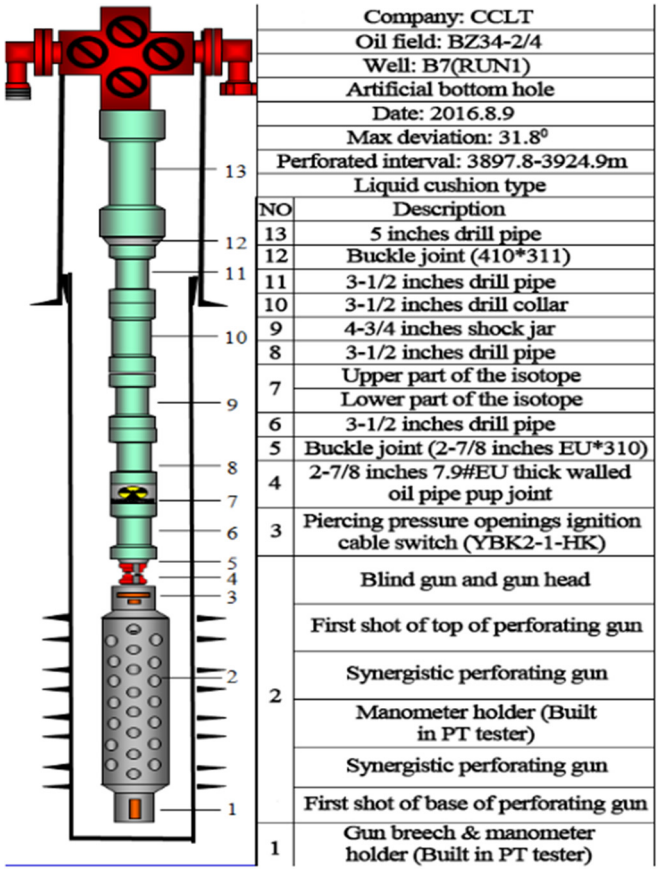

Fig. 4. Schematic diagram of tubular column for perforation.

3.2 Experimental method and optimization

3.2.1 Perforation method and operation process

A sleeve-type composite perforation was used in the experiment, consisting mainly of three parts: the composite perforation device, the P–T test instrument, and the simulation software. The operational process of this field experiment is as follows.

– Assemble the perforation gun at the wellhead; install the sleeve-type composite gunpowder cartridge into the specified position in the perforation gun, and secure it with a guard ring (keeping the slide position).
– Connect the perforation gun.
– Lower it slowly down through the wellhead, preventing the edge of the wellbore from contacting it.
– After passing the perforation device through the wellbore, the remaining procedure is the same as in normal perforation.

3.2.2 Powder charge scheme optimization

Simulation software was used to optimize the charge amount. The preferred results are shown in Tables 2 and 3.

Comparing the above simulation results (Fig. 5), the optimal solution for strata transformation was chosen in order to better measure the pressure curve. The results of the optimal perforation scheme are shown in Table 4.

3.2.3 Experimental safety analysis

Safety of casing: Since certain risks exist in the field experiment, the experimental safety is evaluated. Analysis shows that two factors may damage the casing: perforation holes in the perforation, and pressure generated by the gunpowder inside the casing. Analysis shows that the total number of perforation holes generated this time and the previous time is 32 holes/m, which is not enough to damage the casing. The well casing had been perforated the previous year, and the pressure generated by the gunpowder in this operation is was released to the formation through the holes. Furthermore, the explosion pressure of the system was about 35 MPa, which was far less than the pressure capacity of the 7-inch casing in the perforation section (56.3 MPa), so no pressure problem existed. The cementing quality of this well was good, so the degree of safety was high.

Safety of wellhead pressure: The pressure peak generated after the gunpowder explosion P_m was calculated in the simulation as 129 MPa. After analysis, the wellhead control measures were as follows.

– Prevent the wellhead from sliding, and press with double rings to keep the drill rod from running up.
– Pay close attention to changes in the mud pump pressure gauge. A pressure drop is initiated by the detonator with the open hole. While waiting for delayed detonations, open the valve between the drill rod and the mud pool within 3 minutes, so that the liquid in the drill pipe flows into the mud pool when the fracturing pressure of the gunpowder fluctuates.

Table 2. Simulation results of mantle composite perforation for Sand III formation.

Serial number	1	2	3
Number of fractured segments	2	2	2
Total charge length (m)	16	15	15
(3897.8–3906) m	7	6	7
(3912.8–3924.9) m	9	9	8
Maximum seam length (m)	2.25	2.19	2.13
Maximum slit width (mm)	3.4	3.3	3.2
Skin factor after perforation (relative value)	–2.7	–2.6	–2.6

Table 3. Simulation results of mantle composite perforation of Sand II formation.

Serial number	1	2	3
Number of fractured segments	3	3	3
Total charge length (m)	26.5	26.5	24
(3818.9–3824.6) m	5	4.5	3.5
(3842.6–3844.7) m	1.5	1.5	1.5
(3849.6–3858) m	7	7	5.5
Maximum seam length (m)	2.16	2.15	1.88
Maximum slit width (mm)	3.1	3.1	3.0
Skin factor after perforation (relative value)	–2.6	–2.6	–2.5

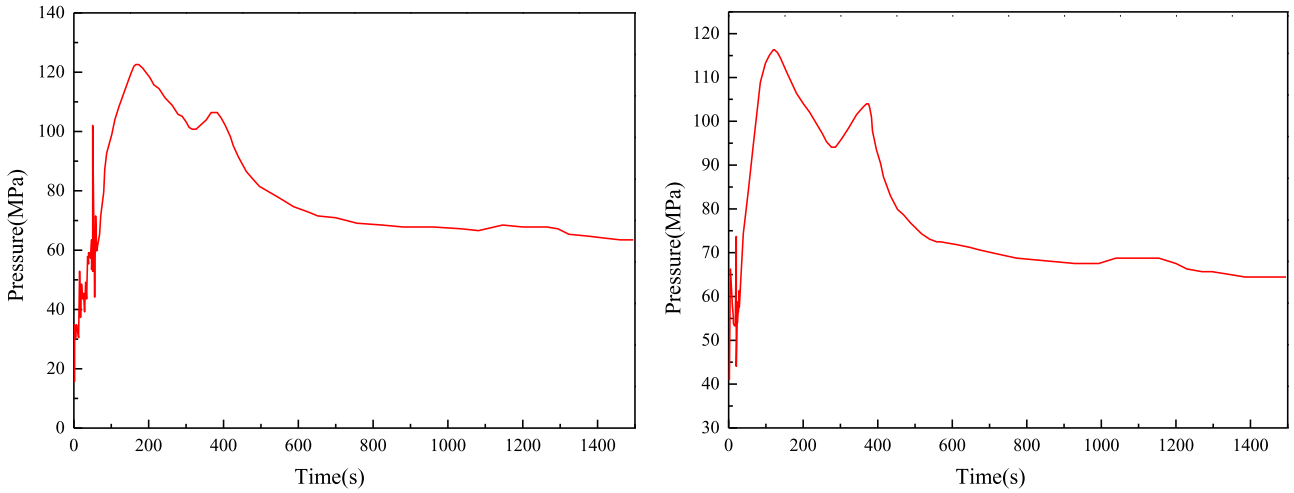

Fig. 5. Simulations of fracture and pressure curves.

– On the production deck, remove the production tree, install the wellhead blowout preventer, kill the well, and open the line connecting the throttle valve to the mud pool.

3.3 Experimental results and perforation load

The field experiment was divided into two groups. The pressure curves around the P–T instrument at the instant of perforation were collected through a high-speed P–T tester installed in the middle of the perforation section, as shown in Figures 6 and 7. The current classic perforation impact load formula is expressed by an approximated exponential decay law (see Josef et al. [26].)

$$p = p_m \cdot e^{-t/\theta}, \tag{10}$$

where p_m is peak pressure, and θ is pressure duration. Therefore, it is necessary to know the pressure peak p_m and pressure duration θ in order to identify the explosion impact load as a function of time. The pressure peak of the explosion shock wave is related to the distance from the explosion center and the charge amount. Spherical TNT charges are generally calculated using the pressure peak formula of underwater explosion shock waves as proposed by Cole et al. [27], shown in detail below

$$p_m = 44.1\left(\frac{W^{1/3}}{R}\right)^{1.5} \tag{11}$$

where p_m is the peak pressure, W is the charge amount, and R is distance from the center of the explosion.

The pressure duration was calculated using the underwater explosion pressure duration proposed by Zamyshlyay et al. [28], as shown below.

$$\theta = 0.084W^{1/3}\left(\frac{W^{1/3}}{R}\right)^{-0.23}. \tag{12}$$

The load curve was calculated using the classic load calculation formula, as shown in Figure 8. Compared with the actual curve, the following deficiencies are found. The

Table 4. Final perforation optimization scheme.

Sand III		Sand II	
Number of fractured segments	2	Number of fractured segments	3
Total charge length (m)	16	Total charge length (m)	13.5
3897.8–3906.4 m	7	3818.9–3824.6 m	5
3912.8–3924.9 m	9	3842.6–3844.7 m	1.5
		3849.6–3858 m	7
Maximum seam length (m)	2.25	Maximum seam length (m)	2.16
Maximum slit width (mm)	3.4	Maximum slit width (mm)	3.1
Skin factor after perforation (relative value)	–2.7	Skin factor after perforation (relative value)	–2.6

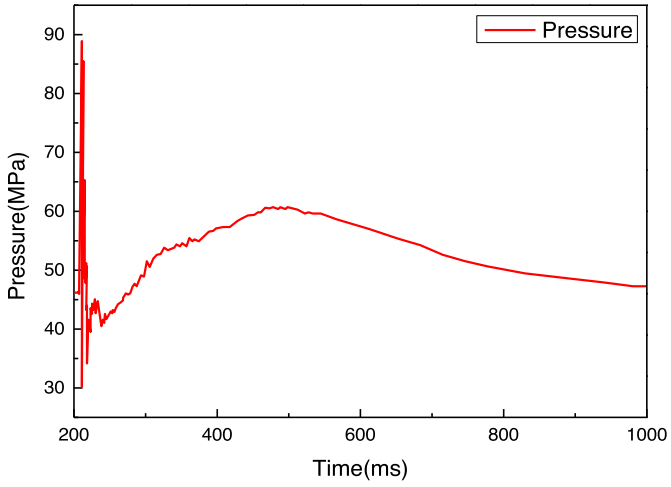

Fig. 6. Pressure curve for Group 1.

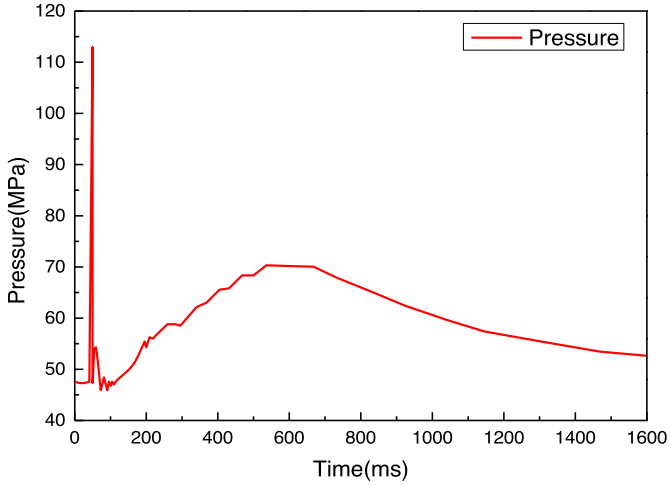

Fig. 7. Pressure curve for Group 2.

actual perforation pressure shows a stage of rising pressure, which continues for some time (generally about 600 ms), and the influence of dynamic forces on the downhole tool is not negligible. The actual pressure eventually tends towards a stable value (mainly caused by the static pressure of the downhole fluid and residual perforation explosion pressure), but the theoretically calculated value

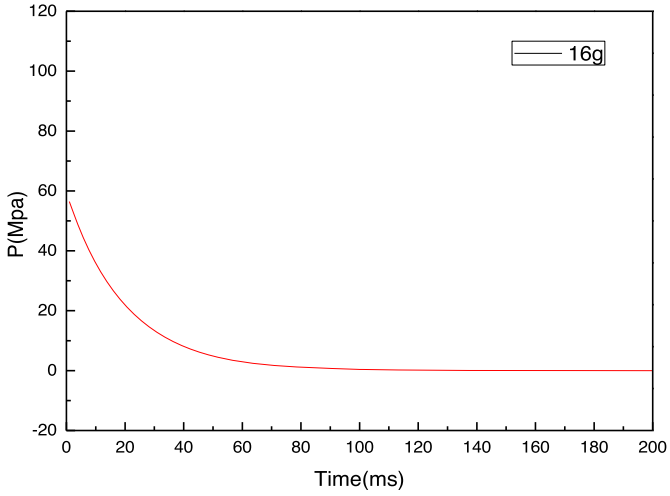

Fig. 8. Pressure curve calculated by the empirical formula shown in formula (11).

tends towards zero. Therefore, based on the above deficiencies, the empirical calculation formula is revised, and a more accurate load calculation formula is obtained as shown in formula (15). The calculated load curve is displayed in Figure 9.

$$p_{(t)} = \begin{cases} \left(\frac{p_m - p_0}{0.6}\right) \cdot t + p_0 (0 \le t < 0.6) \\ p_m \cdot e^{-t/\theta} + p_r (t \ge 0.6) \end{cases} \quad (13)$$

4 Model validation

Commercial software (ANSYS) was used to verify the accuracy of the multiple shock absorber downhole tool dynamic model, as shown in Figure 3. The specific parameters selected are shown in Table 5. The dynamic response of the downhole tool was calculated using ANSYS and the method developed in Section 2, as shown in Figures 10–15.

The displacement and axial force response curves of the downhole tool were calculated using ANSYS and the method developed in Section 2, as shown in the above

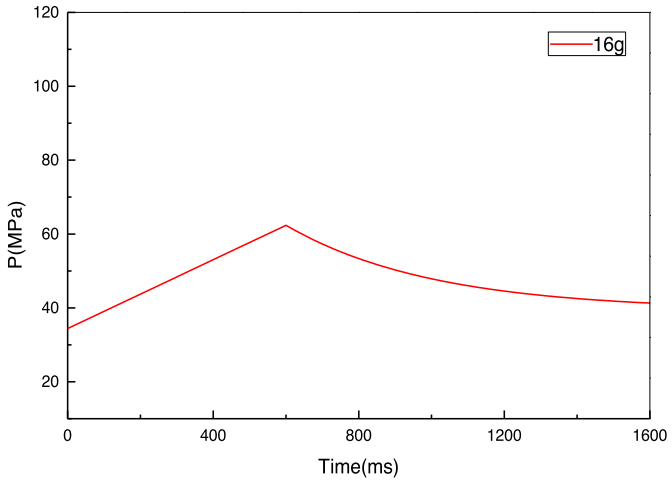

Fig 9. Pressure curve calculated by the formula in this paper.

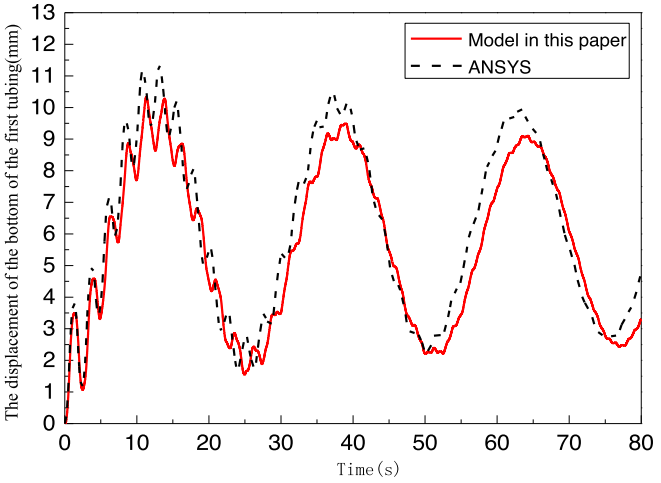

Fig. 10. Displacement diagram of the bottom of the first tubing string.

Table 5. Calculation parameters.

Parameter name	Value
Liquid dynamic viscosity (μ)	0.01 Pa s
Formation pressure gradient	0.96 MPa/100 m
External diameter of oil pipe column	88.9 mm
Internal diameter of oil pipe column	76 mm
Total tube column units	100
Elastic Modulus (E)	2.06×10^{11} Pa
Pipe density (ρ)	7846 kg/m^3
Total calculation time of model	80 s
Step length	0.001 s
Spring stiffness coefficient for a single shock absorber (k)	200 N/mm
Shock absorber damping coefficient (c)	20 N s/mm
Shock absorber mass	100 kg
External diameter of the perforation gun	73 mm
Interior diameter of the perforation gun	62 mm
Perforation gun length	3.3 m
Number of perforation gun dividing units	10
Impact load	0 N

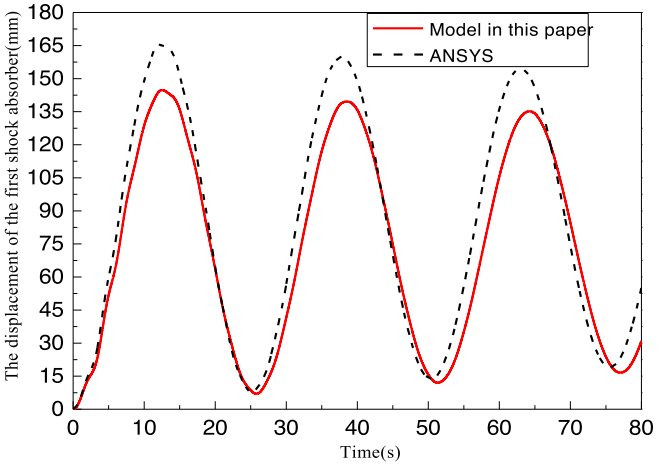

Fig. 11. Displacement diagram of the first shock absorber.

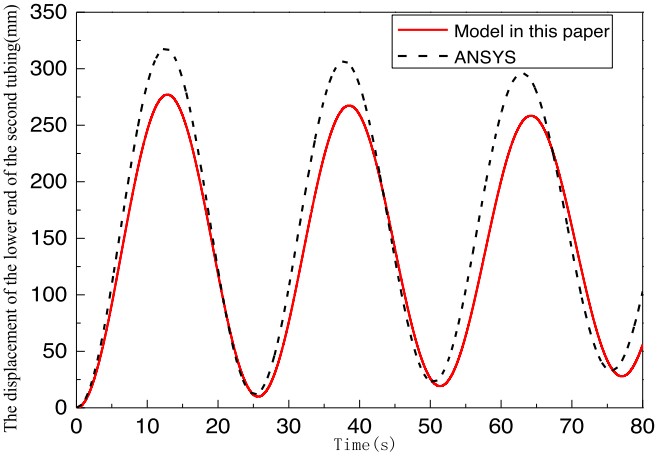

Fig. 12. Displacement diagram of the bottom of the second tubing string.

figures. These figures show that the results calculated by ANSYS is essentially the same as that obtained by the model in this paper, demonstrating its accuracy and providing a theoretical basis for the following study of downhole tool dynamic characteristics.

5 Effects of shock absorbers on the dynamic characteristics of downhole tools

The dynamic response of the downhole tools was calculated using Fortran programming, with the specific parameters shown in Table 6. The impact pressure field in the wellbore

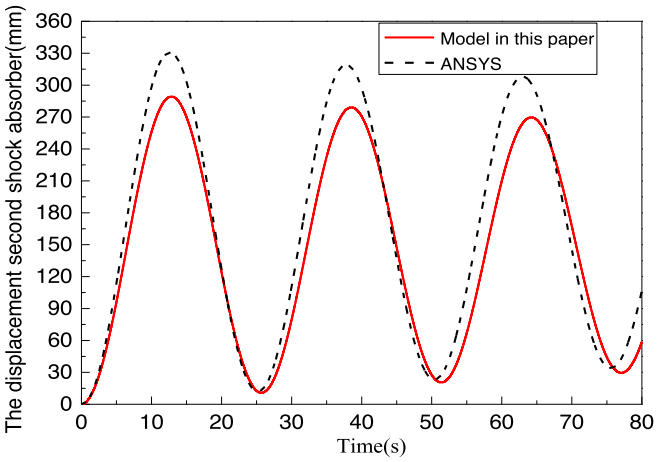

Fig. 13. Displacement diagram of the second shock absorber.

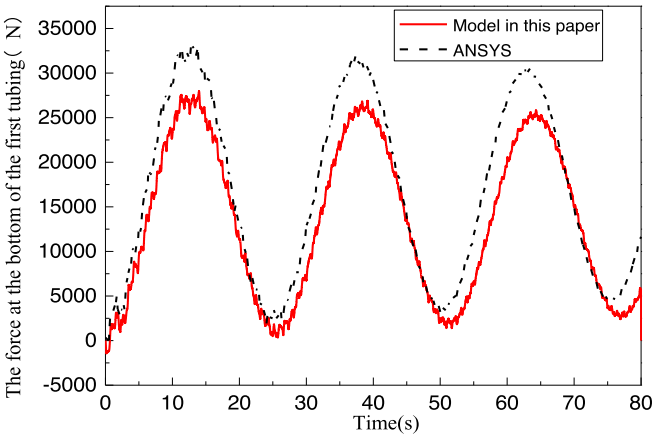

Fig. 15. Axial force diagram of the bottom of the first tubing string.

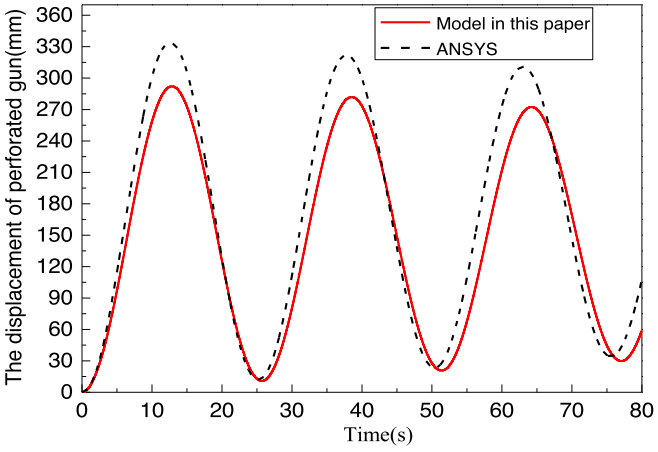

Fig. 14. Displacement diagram of the bottom of the perforation gun.

was calculated using the method developed in Section 3, and the multiple shock absorber downhole tool dynamic model is shown in Figure 3.

5.1 Effects of shock absorbers on the displacement and axial forces

In the example calculation parameters, the length of the tubing string is 200 m, and a uniform configuration was applied for the shock absorber. The different shock absorbers were set to the same stiffness and damping settings. The dynamic response of the downhole tools is calculated as shown in the following figure.

Figures 16–18 show the displacement diagrams of the bottom of the first, second, and third tubing string, going down from the top. Analysis of the displacement amplitude on the same positions in these figures shows that it decreases significantly as the number of shock absorbers increases from one to two, but the decrease is very significant when the number increases from two to three. The change in vibration frequency for the first tubing string is not significant with the increase, while the vibration frequencies of the second and third tubing strings are significantly reduced. Analysis on the changes of the axial force curves in Figures 19–21, and on the change of the axial force curves in different positions, shows that the axial force amplitude of the first tubing string is much larger than that of the second one. This is because the closer to the upper end of the tubular column, the more it bears the

Table 6. Basic parameters for downhole tool dynamic analysis.

Parameter name	Value
Liquid dynamic viscosity (μ)	0.01 Pa s
Formation pressure gradient	0.96 MPa/100 m
Oil column yield strength limit (σ_s)	758 MPa
External diameter of oil pipe column	88.9 mm
Internal diameter of oil pipe column	76 mm
Total number of oil column units	100
Elastic modulus (E)	2.06×10^{11} Pa
Pipe density (ρ)	7846 kg/m^3
Total calculation time of model	80 s
Step length	0.001 s
Spring stiffness coefficient for a single shock absorber (k)	200 N/mm
Shock absorber damping coefficient (c)	20 N s/mm
Shock absorber mass	100 kg
External diameter of the perforation gun	73 mm
Internal diameter of the perforation gun	62 mm
Perforation gun length	3.3 m
Number of perforation gun dividing units	10
Charge amount	128 g
Distance to explosive center	0.2 m
Hydrostatic pressure	34.4 MPa
Critical strength factor for casing	98.9 MPa

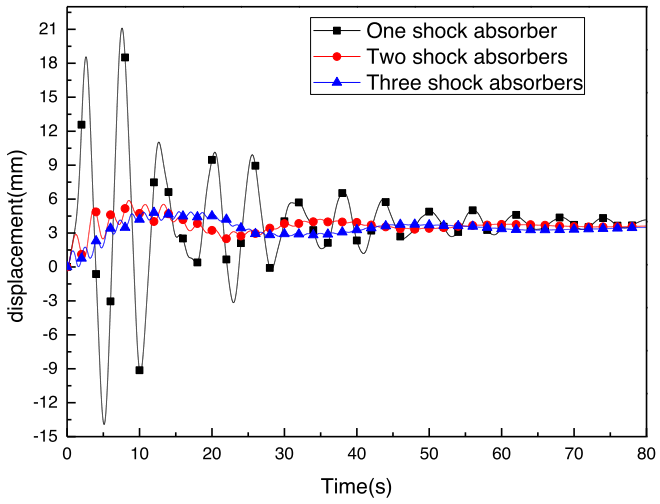

Fig. 16. Bottom displacement of the first tubing string.

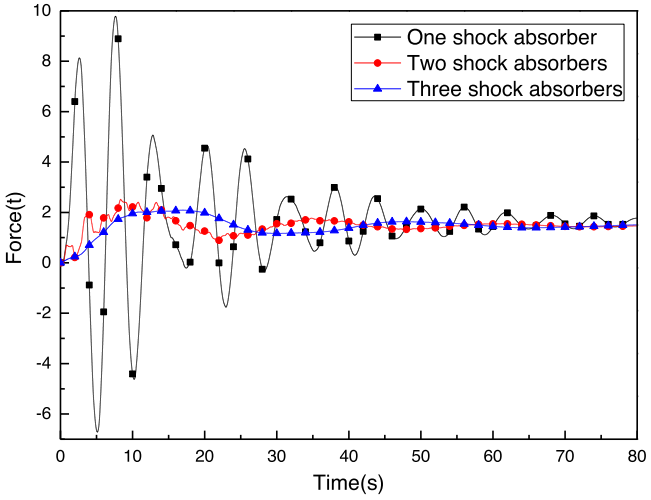

Fig. 19. Axial forces on the bottom of the first tubing string.

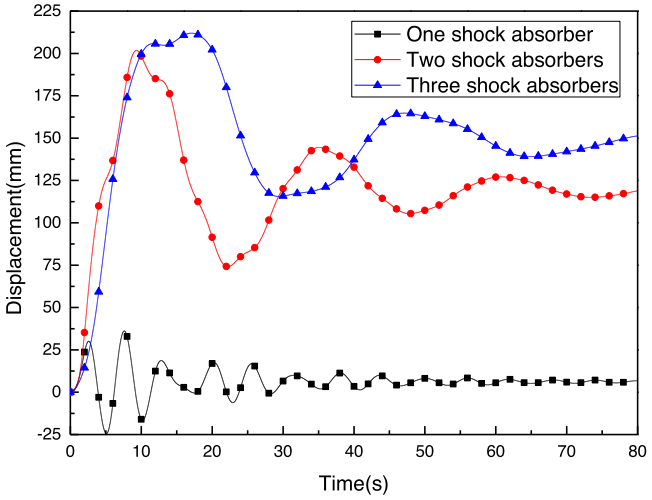

Fig. 17. Bottom displacement of the second tubing string.

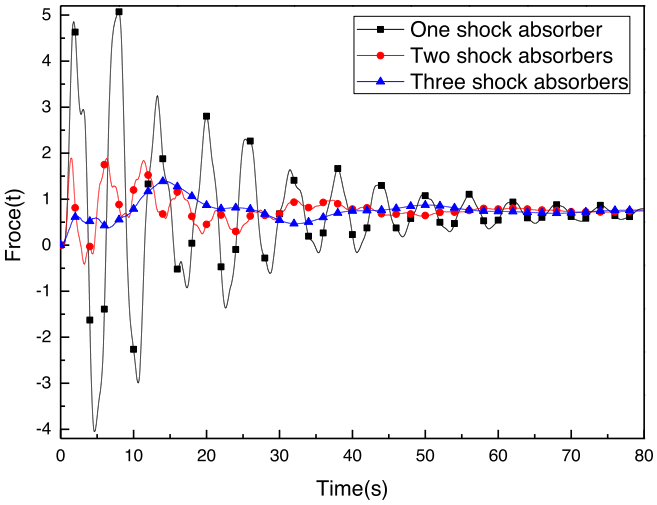

Fig. 20. Axial forces on the bottom of the second tubing string.

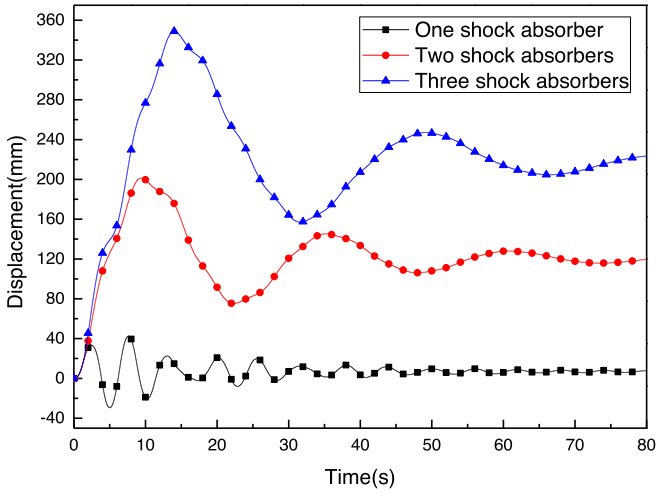

Fig. 18. Bottom displacement of the third tubing string.

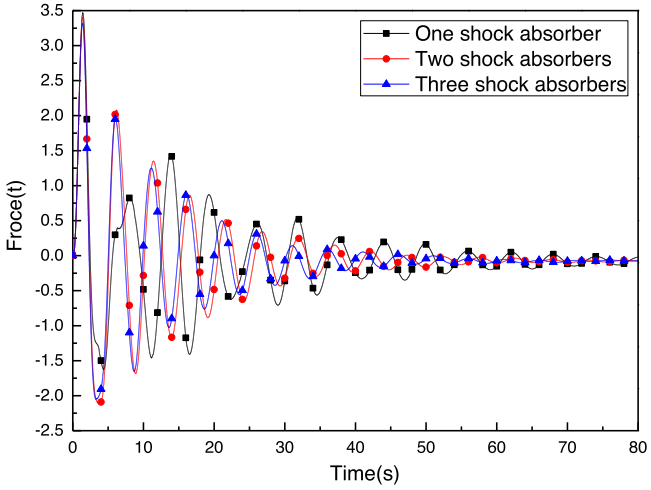

Fig. 21. Axial forces of the bottom of the third tubing string.

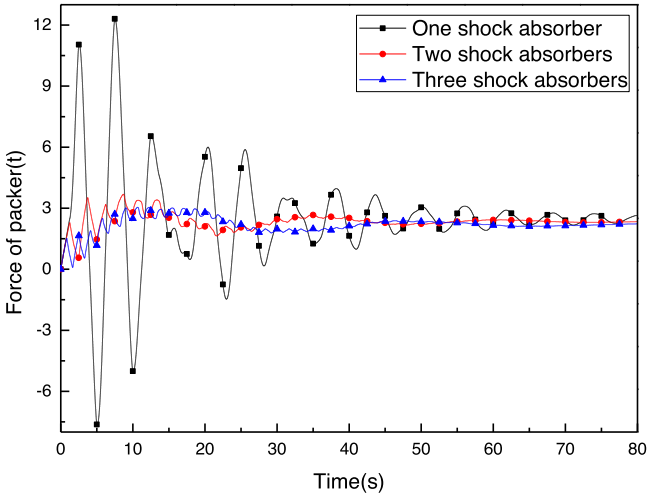

Fig. 22. Force of packer.

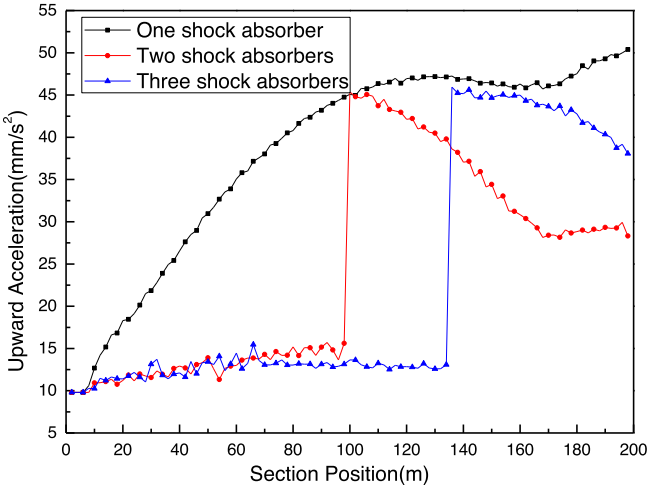

Fig. 23. Maximum upward acceleration in each section.

weight of the tubular column and the shock absorber. The axial force curves of the tubing string from the same position show that the axial force amplitude decreases from 10 t to about 2 t as the number of shock absorbers increases from one to two, and the difference is significant. However, the decrease in axial force amplitude is not significant when the number of shock absorbers changes from two to three. Therefore, two shock absorbers can be used at different positions to reduce damage from perforation hole impact loads to the tubular column; the use of three or more shock absorbers, on the other hand, has no significant effect on damping.

5.2 Effects of shock absorbers on force of the packer and acceleration of tubing string

The force change curves in Figure 22 show that the force reaches a portion of the packer's unsealing force (12 t) with a single shock absorber at a charge of 128 g, and accidents involving premature packer unsealing may occur. With two shock absorbers, the force on the packer is significantly reduced, however the decrease is not significant with three. Therefore, two shock absorbers can be set in different positions of the tubular column to achieve the desired perforation effect, but it is not necessary to use three. The effect of the shock absorbers on the maximum acceleration of each tubular column cross-section is displayed in Figures 23 and 24. They show that the acceleration speed of the upper tubular column decreases significantly as the number of shock absorbers increases, while the change in the lower tubular column is moderate. The decrease in acceleration in the upper tubular column is not significant when the number of shock absorbers is increased from two to three, but acceleration in the lower tubular column increases. Therefore, the test equipment of the tubular column is preferably installed on its upper section. Two shock absorbers should be used, but it is not necessary to install too many. When the test instrument must be set at the lower end, the number of shock absorbers should still be two.

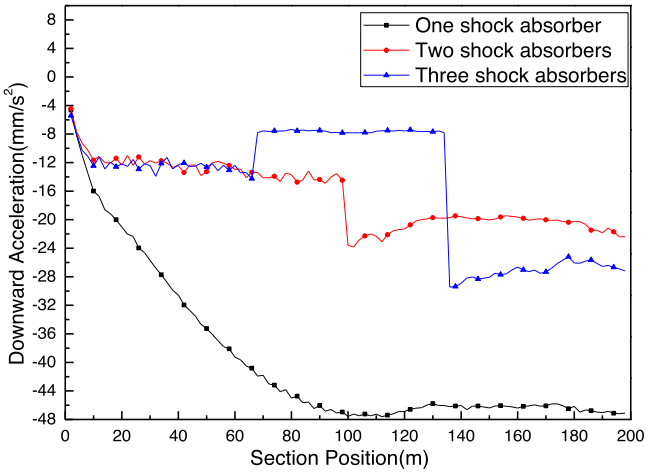

Fig. 24. Downward acceleration in each section.

5.3 Effects of shock absorbers on tubing string buckling

To analyze the stability of the tubing string, the external tubing string diameter of the perforation section is set as d_o, the inner diameter as d_i, and the maximum pressure generated the by explosion shock wave in each cross-section of the tubing string as p_t. Then the upward load to which the tubing string is subjected at the moment of perforation is as follows (see Ni [29]).

$$F_A = \frac{\pi}{4} p_t \left(d_o^2 - d_i^2\right). \tag{14}$$

According to the formula to calculate the critical tubing string helical buckling load,

$$F_{\text{crh}} = 5.55 \sqrt[3]{EIq^2} \tag{15}$$

where E is the tube's elastic modulus, and I is its transverse moment of inertia.

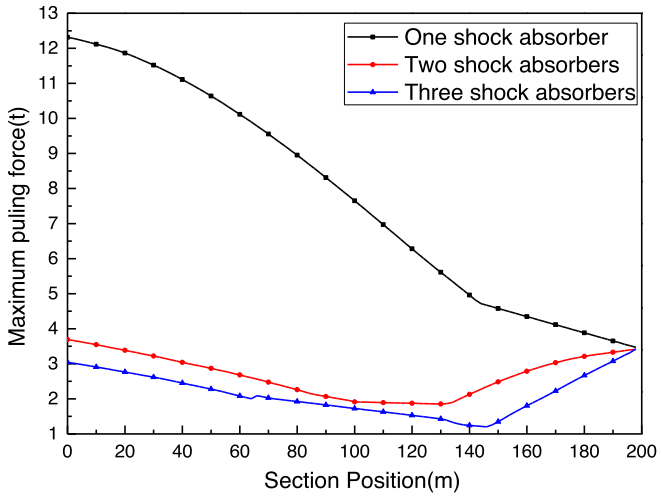

Fig. 25. Maximum downward axial force in each cross-section.

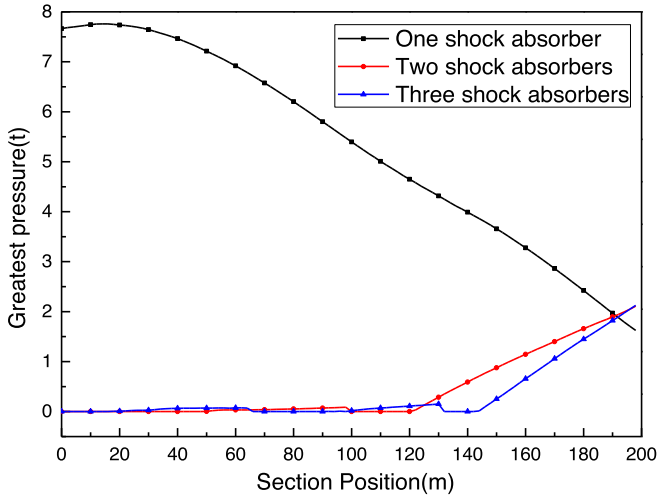

Fig. 26. Maximum upward axial force in each cross-section.

According to formulas (14) and (16), if $F_A > F_{crh,}$ we know that the tubing string will undergo helical buckling under the action of the impact load, otherwise helical buckling does not occur. In the present study, we mainly consider the case where it occurs. If the tubing string undergoes helical buckling, then it comes into contact with the casing, making it difficult or even impossible to remove the tubing string. Based on the above theory, the axial force and stability safety factors for each section of the tube are calculated as shown in the following figures.

The effect of the number of shock absorbers on the axial force and buckling deformation of each cross-section of the tubing string is shown in Figures 25 and 26. The figures show that the maximum axial force in each cross-section near the upper 2/3 section of the oil pipe decreases significantly as the number of shock absorbers increases from one to two; however when the number of shock absorbers increases from two to three, the change in axial force is not significant. At the same time, the axial force of the tubular column bottom increases, and finally reaches

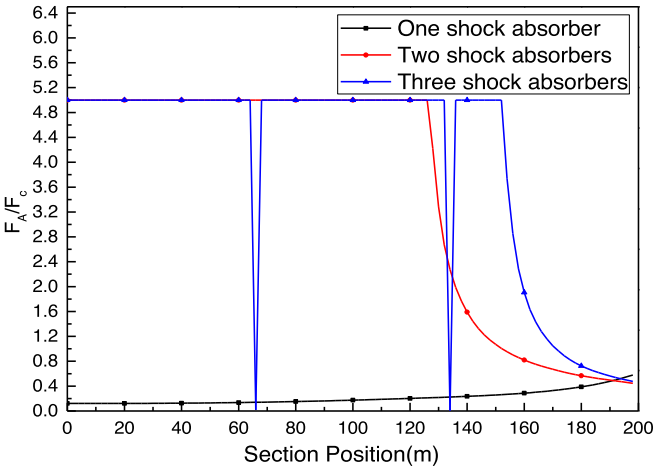

Fig. 27. Tubing string buckling.

the same value as the bottom of the tubular column. In Figure 27, F_A is the critical load for helical buckling deformation of the tubular column, F_A is the maximum axial force of each section of the tubular column, and Pc ($=F_A/F_{\mathrm{crh}}$) is the factor to determine whether or not the tubular column undergoes buckling deformation. When $P_c \geq 1$, helical buckling does not occur; when $P_c < 1$, it occurs; when $P_c > 5$, everything is set to 5. Therefore, with one shock absorber, helical buckling deformation may occur in all sections of the tubular column; when the number increases to two, most positions near the upper end of the tubular column do not undergo helical buckling, and the buckling occurs only on the lower end. When the number is increased to three, some places instantly become 0, due to negligible force at the junctions, and even fewer positions of the column experience helical buckling. Thus, increasing the number of shock absorbers reduces the number of helical buckling positions in the tubular column.

5.4 Effects of shock absorbers on the stress of tubing string

During perforation, the tubing string is not only impacted by internal and external fluids, but is also subjected to explosion shock pressure generated by the perforation explosions, among other factors. Because the tubing string is affected by all kinds of pressure, the probability of its damage is greatest, so it is critical to analyze its strength. Because the tube is subjected to pressure in three directions, a fourth theoretical strength analysis is necessary. The specific formula is shown in Xu [30] as follows:

$$\sigma_{xd4} = \sqrt{\frac{1}{2}\left[(\sigma_z - \sigma_\theta)^2 + (\sigma_\theta - \sigma_r)^2 + (\sigma_r - \sigma_z)^2\right]} \quad (16)$$

$$K_{xd} = \frac{\sigma_s}{\sigma_{xd4}} \quad (17)$$

where K_{xd} is the triaxial stress safety factor, σ_s is the yield stress of the tubing string (MPa), and σ_{xd4} is the equivalent stress (MPa).

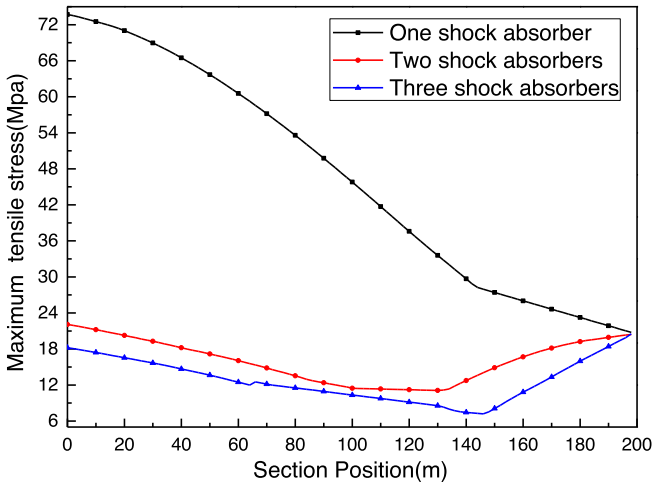

Fig. 28. Maximum tensile stress of each section.

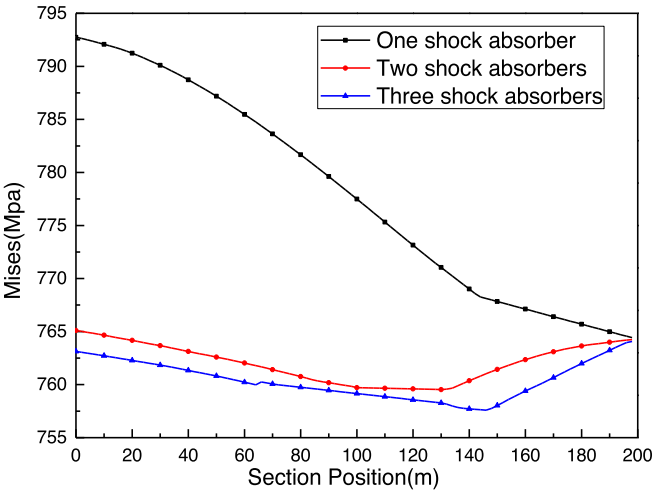

Fig. 30. Mises stress of each section.

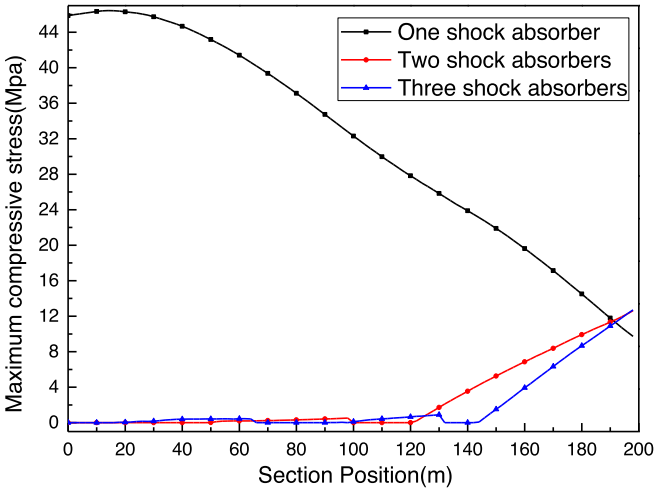

Fig. 29. Maximum compressive stress of each section.

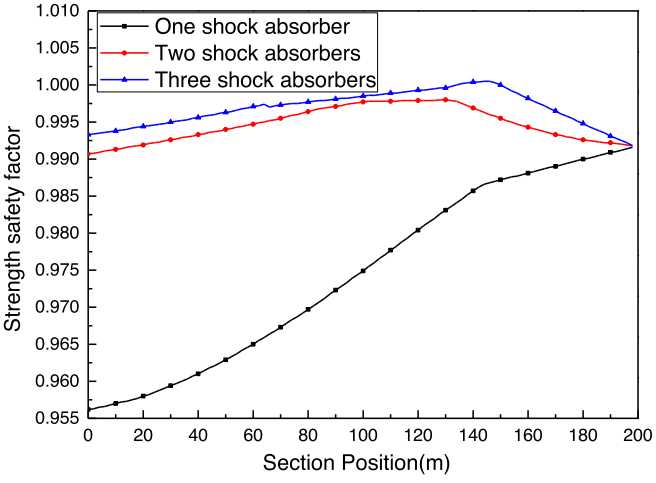

Fig. 31. Strength of each section.

The pressure and axial force of each section can be calculated through the above calculation formula in Section 3, then the maximum equivalent stress of different sections of tubular column can be calculated to obtain the safety coefficient curve of the tubing string. Based on the above basic theory, the example parameters shown below are used to calculate the equivalent stress and strength safety factors.

Figures 28 and 29 show the maximum tensile compressive stress curves for each section of the tubing string. The figures show that as the number of shock absorbers is increased from one to two, the stress decreases significantly towards the upper portion of the tubing string. When two shock absorbers are used, the axial force at the lower end of the tubing string increases. When the number is increased to three, the axial force on the tubing string does not change significantly. Figure 30 shows the Mises stress curve of each section of the tubing string. Its characteristics are similar to those of tensile stress. Therefore, the Mises stress change of the tubing string is mainly caused by its tensile stress. The Mises stress reduction amplitude of the tubing string is not very large, mainly because of the effects of external pressure (the shock wave generated by the impact load). Figure 31 shows the strength safety coefficients curves of each tube section, demonstrating that the tubing string is greatly damaged by the shock wave generated by the impact load when a single shock absorber is used, and the charge amount is 128 g. Increasing the number of shock absorbers improves the safety coefficient of the tubing string, and no damage occurs in some positions. Therefore, the effect of the increase on tubing string damage is not significant, and other methods are also required to achieve that purpose.

6 Discussion and conclusions

The influence mechanism of the number of shock absorbers on the dynamic behavior of downhole tool vibration

problems during perforation has been studied, and the following conclusions have been obtained.

- Based on analysis of the downhole tool structure, a multiple shock absorber downhole tool dynamic model has been established for perforation operations. The multi-level tubing string-shock absorber-perforation gun coupling, the fluid damping, and the weight of the tubing string were all considered, and the accuracy of the model was verified using commercial software (ANSYS).
- Perforation impact load field tests were conducted, and pressure curves were measured in the example well. By comparing the actual pressure curve with that calculated from engineering load formulae, a more realistic load calculation formula was obtained, providing a more accurate load calculation method to study downhole tool dynamic responses.
- The effects of different numbers of shock absorbers on the dynamic characteristics of the downhole tool were also analyzed. The force of the packer reached the unsealing point during perforation when the charge was 128 g and a single shock absorber was used, but its force was significantly reduced as the number of shock absorbers increased. The acceleration of the upper tubing string decreased significantly as the number increased, so the test instrument is preferably installed on the upper portion of the tubing string. With more shock absorbers, the axial force on each section of the tube decreased, and fewer positions on the tubing string experienced helical buckling. Therefore, the use of multiple shock absorbers at different positions of the tube can reduce the possibility of helical buckling. When the length of the tubing string was 200 m, the effect of the two shock absorbers was significant. The effect decreased with additional shock absorbers. Therefore, the length of the tube determines the optimal number to install.

Conflicts of interest. The authors declare no conflicts of interest regarding the publication of this paper.

Acknowledgments. This work has been supported in part by National Natural Science Foundation of China (Grant No. 51875489) and Open Fund of Key Laboratory of Oil & Gas Equipment, Ministry of Education (Southwest Petroleum University) (Grant No. OGE201701-01).

References

[1] W.X. Liu, P. Zhang, Reliability analysis of downhole tool, Oil Field Equip. **38**, 56–59 (2009)
[2] J.G. Ning, Explosion and Impact dynamics, National Defense Industry Press, Beijing, 2010
[3] X.J. Ren, J.H. Wang, Numerical Simulation Technology of Shallow Water Explosion in Group Charge, West. Min. Eng. **20**, 125–127 (2005)
[4] C.B. Li, Y. Liang, Engineering calculation and application of perforation impact dynamic loads in oil and gas well, Adv. Mater. Res. **834–836**, 1308–13012 (2014)
[5] W.B. Zhang, S. Xie, Impact analysis of perforation-acidification-test-tube column by perforating impact loading, Oil Gas Well Test **25**, 8–11+73 (2016)
[6] K. Lu, B.H. Li, Numerical simulation and experimental Study of equal aperture perforation projectile, Logging Technol. **03**, 024 (2017)
[7] W.Q. Pan, D.X. Fu, Study on perforation performance of double-layer liner with energy perforating projectile, Blast. Equip. **02**, 007 (2017)
[8] J. Liu, S.D. Li, Study on dynamic response of downhole tools under perforation impact load, Shock Vib. **10**, 1155 (2017)
[9] A. Lubinski, A study of the buckling of rotary drilling string, Drill Prod. Pract. **34**, 178–214 (1950)
[10] A. Lubinski, W.S. Althouse, J.L. Logan, Helical buckling of tubing sealed in Parker, JPT **14**, 655–667 (1962)
[11] K.G. Sorenson, Post-buckling behavior of circular rod constrained within a circular cylinder, Trans. ASME **53**, 929–934 (1986)
[12] Z.J. Cui, H.P. Hu, Y.T. Hu, Dynamic analysis of shock absorber considering deformation effect of upper tubular column, Hua Zhong Univ. Sci. Technol. **36**, 106–108 (2008)
[13] F. Chen, H.B. Chen, Influence of perforation impact load on working string and its countermeasures, Dev. Eng. **30**, 61–65 (2010)
[14] Z.F. Li, Y.T. Cai, D.M. Li, Mechanical analysis of pipe string in formation testing, Acta Petrol. Sin. **32**, 709–716 (2011)
[15] X.T. Yang. F.X. Zhang, M.F. Li, Y.H. Dou, Analysis of strength safety of perforated string considering detonation parameters, Adv. Mater. Res. **634–638**, 3573–3576 (2013)
[16] H.F. Zhou, Research on the dynamic response of the oil well perforating string to explosive impact load, Beijing Institute of Technology, 2014
[17] C. Huang, Study on dynamic behavior of deep water test tube under impact load, Southwest Petroleum University, 2015
[18] W.J. Huang, D.L. Gao, Y.H. Liu, A study of tubular string buckling in vertical wells, Int. J. Mech. Sci. **118**, 231–253 (2016)
[19] B.Y. Wang, D.L. Gao, J. Fang, Assessment of wellbore integrity of offshore drilling in well testing and production, Am. Soc. Civil Eng. **142**, 1943–7889 (2016)
[20] W.J. Huang, D.L. Gao, A Local Mechanical Model of Down-Hole Tubular strings and its Amendment on the integral Model, SPE-180613-MS
[21] Z.F. Li, C.Y. Zhang, G.M. Song, Research advances and debates on tubular mechanics in oil and gas wells, J. Petrol. Sci. Eng. **151**, 194–212 (2017)
[22] C. Ke, X. Song, Computationally efficient down-hole drilling system dynamics modeling integrating finite element and transfer matrix, J. Dyn. Syst. Measur. Control **139**, 121003 (2017)
[23] T. Feng, I. Kim, D. Chen, Dynamic modeling of directional drillstring: a linearized model considering well profile, J. Dyn. Syst. Measur. Control **140**, 061005 (2018)
[24] T. Feng, S. Bakshi, Q. Gu, D. Chen, A finite element modeling framework for curved beam dynamics considering nonlinearities and contacts, J. Comput. Nonlinear Dyn. **14**, 081003 (2019)

[25] K.L. Nguyen, Q.T. Tran, M.-A. Andrianoely, L. Manin, R. Dufour, S. Menand, M. Mahjoub, Campbell diagram computation for a drillstring immersed in curved wells, J. Vib. Acoustics **141**, 041009 (2019)
[26] H. Josef, The dynamics of explosion and its use, Elsevier Scientific Publishing Company, Amsterdam, Oxford, New York, 1984
[27] Cole, Underwater explosion, 1960
[28] B.V. Zamyshlysaev, Dynamic Loading in Underwater Explosion. AD-7571 3, 1973
[29] Z.H. Ni, Vibration Dynamics, Xi an Jiao tong University Press, Xi an, 1989
[30] Z.L. Xu, Elasticity mechanics Next volume, Higher Education Press, Beijing, 2006

Cite this article as: X. Guo, J. Liu, G. Wang, Q. Liu, X. Song, Investigation into the dynamic characteristics of downhole perforation tools with multiple shock absorbers, Mechanics & Industry **20**, 622 (2019)